

# Nanoscale

Accepted Manuscript



This is an *Accepted Manuscript*, which has been through the Royal Society of Chemistry peer review process and has been accepted for publication.

*Accepted Manuscripts* are published online shortly after acceptance, before technical editing, formatting and proof reading. Using this free service, authors can make their results available to the community, in citable form, before we publish the edited article. We will replace this *Accepted Manuscript* with the edited and formatted *Advance Article* as soon as it is available.

You can find more information about *Accepted Manuscripts* in the [Information for Authors](#).

Please note that technical editing may introduce minor changes to the text and/or graphics, which may alter content. The journal's standard [Terms & Conditions](#) and the [Ethical guidelines](#) still apply. In no event shall the Royal Society of Chemistry be held responsible for any errors or omissions in this *Accepted Manuscript* or any consequences arising from the use of any information it contains.

## COMMUNICATION

## $^{201}\text{Tl}^+$ -labelled Prussian Blue Nanoparticles as Contrast Agents for SPECT scintigraphy

Cite this: DOI: 10.1039/x0xx00000x

M. Perrier,<sup>a</sup> M. Busson,<sup>b\*</sup> G. Massasso,<sup>a</sup> J. Long,<sup>a</sup> V. Boudousq,<sup>c</sup> J.-P. Pouget,<sup>c</sup> S. Peyrottes,<sup>d</sup> Ch. Perigaud,<sup>d</sup> C. Porredon-Guarch,<sup>e</sup> J. de Lapuente,<sup>e</sup> M. Borrás,<sup>e</sup> J. Larionova,<sup>a\*</sup> and Yannick Guari<sup>a</sup>

Received 00th January 2012,  
Accepted 00th January 2012

DOI: 10.1039/x0xx00000x

www.rsc.org/

**Prussian blue (PB) and its analogues at the nanometric scale are exciting nano-objects that combine the advantages of molecular-based materials and nanochemistry. Herein, we demonstrate that ultra-small PB nanoparticles of 2–3 nm can be easily labelled with radioactive  $^{201}\text{Tl}^+$  to obtain new nanoprobes as radiotracers for 201-thallium-based imaging.**

Cyano-bridged coordination polymers also known under the name Prussian Blue (PB) and its analogues (PBA) have been extensively investigated over the past four decades due to their exciting magnetic, photo-switchable and intercalation properties as well as for their technological applications as pigment, molecular sieve or for hydrogen storage.<sup>1</sup> PB has the general formula  $A_{x/4}[\text{Fe}(\text{CN})_6]_{1-x/4}$  ( $A$ , monovalent cation;  $\square$  hexacyanoferrate vacancy) and its structure consists in a face-centered cubic structure where Fe(II) and Fe(III) ions are connected *via* cyano bridges leading to a three-dimensional open-framework that allows the intercalation of cations. Remarkably, bulk PB and PBA are effective and selective sorbents for the capture of  $\text{Cs}^+$  and  $\text{Tl}^+$  ions which makes these compounds extremely interesting for decontamination procedures of the different isotopes of these ions, radioactive or not, and their use as antidotes.<sup>2</sup> Recently, a major effort of the research activity on PB and PBA has been focused on their investigation at the nanometric scale. A wide variety of PBA based nano-objects of different chemical composition, size, shape and of tuneable surface properties have been reported.<sup>3</sup> Among these, a particular attention was paid to the design of nano-sized materials stabilized in aqueous solution with biocompatible stabilizing agents for biomedical applications.<sup>4–7</sup> This, nanoparticles (NPs) of PB and certain of its analogues were found promising as potential contrast agent for different types of imagery including Magnetic Resonance Imaging,<sup>4</sup> computed tomography,<sup>5</sup> as optical biomarkers<sup>6</sup> or as therapeutic agents.<sup>7</sup> However, such NPs were never employed as a carrier of radioisotopes for the design of nano-radiotracer for Single-Photon Emission Computed Tomography imaging (SPECT).

$^{201}\text{Tl}$ -based SPECT constitutes a powerful diagnostic technique widely used in nuclear medicine, wherein the radioisotope is internalized and the emitted radiation is captured by an external detector. More than two decades ago,  $^{201}\text{Tl}^+$  was the only radioactive element available to clinicians for myocardial imaging and, despite the appearance of  $^{99\text{m}}\text{Tc}$ , remains extensively used for different types of myocardial diagnostics, by intravenous (*iv*) administration of an aqueous TlCl

solution.<sup>8</sup> In this case, about 90 % of radioactive thallium ions are cleared from the blood after the first cycle of circulation and only 10 % of the injected activity is used for imaging. In this article, we report the design of ultra-small  $^{201}\text{Tl}$ -labelled PB NPs stabilized by glucose functionalized aminotriethyleneglycol ( $\beta$ -GluTEG-NH<sub>2</sub>) or aminopolyethylene glycol (PEG-NH<sub>2</sub>), which can be used as nanocarriers of radioactive  $^{201}\text{Tl}^+$  and their potential use as radio nanoprobes for *in vivo* SPECT/Computed Tomography (CT) imaging. These NPs present : (i) a combination of an ultra-small size (< 5 nm) of the inorganic cyano-bridged core with compatible ligands made from glycol chains and/or carbohydrates covalently anchored *via* functional amino groups at their surface providing the possibility of prolonged blood circulation and glomerular clearing; (ii) an excellent hydrosolubility to

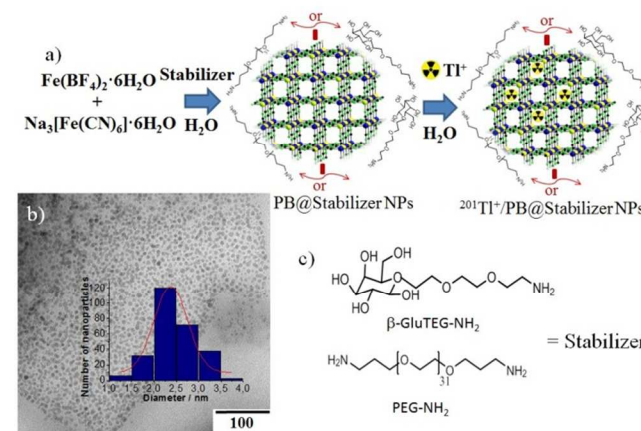


**Figure 1.** a) Schematic representation of the PB@stabilizer and  $^{201}\text{Tl}^+/\text{PB}@$ stabilizer nanoparticles synthesis; b) TEM image of the  $\text{Na}_{0.45}\text{Fe}[\text{Fe}(\text{CN})_6]_{0.86}@\text{(PEG-NH}_2\text{)}_{0.22}$  nanoparticles and the corresponding histograms of the nanoparticles' size distribution (inset) and c) Schematic representation of the stabilizers ( $\beta$ -GluTEG-NH<sub>2</sub> and PEG-NH<sub>2</sub>) used.

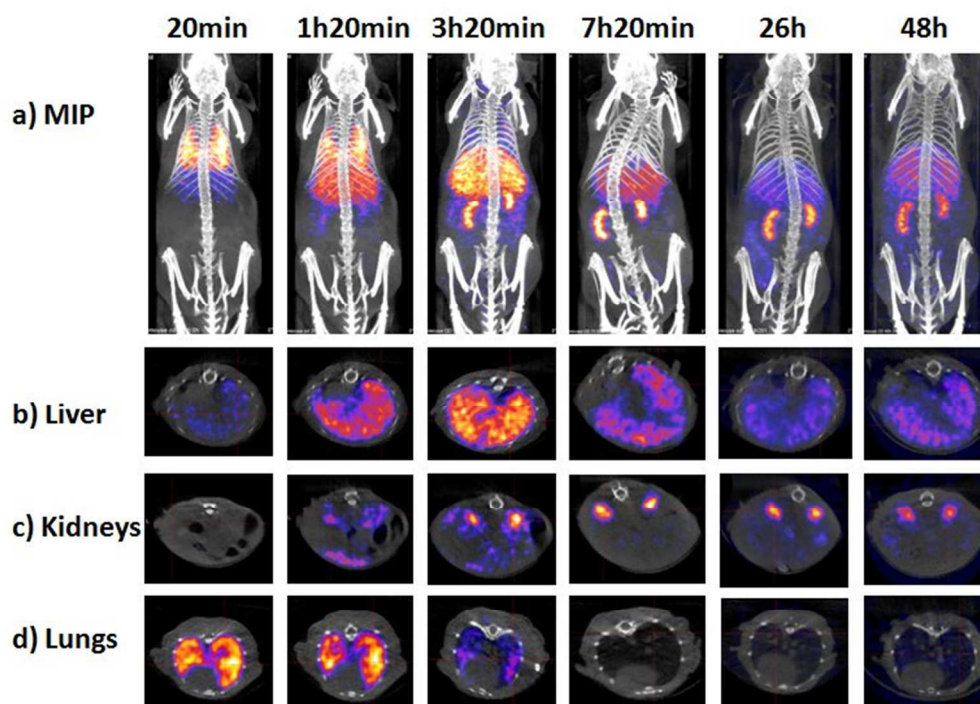


**Figure 2.** SPECT/CT images of the mice after *iv* injection of the  $^{201}\text{Tl}^+$ /PB@PEG-NH<sub>2</sub> nanoparticles for different periods of time: 20 min, 1h20, 3h20, 7h20, 26h and 48h with a) Maximum Intensity Projection (MIP) and transversal planes showing different organs of interest b) liver, c) kidneys and d) lungs.

yield very stable colloidal solutions in water; (iii) radioactive  $^{201}\text{Tl}^+$  entrapped within the PB network, which make them effective nanocarriers of this monovalent ion.

The  $^{201}\text{Tl}^+$ -nanocarriers were obtained by a two-step approach comprising first the synthesis of sodium-containing PB NPs in aqueous solution by a self-assembly reaction of the two molecular precursors,  $\text{Na}_3[\text{Fe}(\text{CN})_6]$  and  $\text{Fe}(\text{BF}_4)_2 \cdot 6\text{H}_2\text{O}$ , in the presence of the biocompatible stabilizer ( $\beta$ -GluTEG-NH<sub>2</sub> or PEG-NH<sub>2</sub>) and then the post-synthetic sequestration of  $^{201}\text{Tl}^+$  (Fig. 1). The stabilizer,  $\beta$ -GluTEG-NH<sub>2</sub>, was prepared in three steps from 2-[2-(2-chloroethoxy)ethoxy]ethanol and penta-acetyl-D-glucose, in 64 % overall yields (see ESI). The sodium PB@stabilizer NPs obtained after the first step of the synthesis whose formulas are  $\text{Na}_{0.44}\text{Fe}[\text{Fe}(\text{CN})_6]_{0.85} @ (\beta\text{-GluTEG-NH}_2)_{0.60}$  and  $\text{Na}_{0.45}\text{Fe}[\text{Fe}(\text{CN})_6]_{0.86} @ (\text{PEG-NH}_2)_{0.22}$  present the structural characteristics of the bulk PB as attested by the stretching vibration of the cyano group<sup>9</sup> at *ca.* 2070  $\text{cm}^{-1}$  as well as their powder X-Ray diffraction (PXRD) patterns (Figure 1S, ESI).<sup>10</sup> The presence of the stabilizing agents in both cases was confirmed by the observation of C-H stretching vibrations bands in the 2800-2950  $\text{cm}^{-1}$  region. Transmission Electronic Microscopy (TEM) analysis reveals the formation of ultra-small non-aggregated spherical NPs with a mean size distribution of  $2.4 \pm 0.5$  nm for  $\text{Na}_{0.45}\text{Fe}[\text{Fe}(\text{CN})_6]_{0.86} @ (\text{PEG-NH}_2)_{0.22}$  (Fig. 2) and  $2.4 \pm 0.6$  nm for  $\text{Na}_{0.41}\text{Fe}[\text{Fe}(\text{CN})_6]_{0.85} @ (\beta\text{-GluTEG-NH}_2)_{0.60}$  (Fig. 2S, ESI), respectively. Note that the NPs are readily redispersible in water or in physiological solution, and the corresponding solutions remain stable for several weeks. At the second step, the thallium ions were inserted into the cyano-bridged

network of PB by simply mixing the PB@stabilizer NPs with  $\text{TlCl}$  in aqueous solution. Study of the  $\text{Tl}^+$  capture was first investigated by using a non-radioactive isotope in water. The sorption kinetic curve performed for  $\text{Na}_{0.45}\text{Fe}[\text{Fe}(\text{CN})_6]_{0.86} @ (\text{PEG-NH}_2)_{0.22}$  by using an aqueous solution of  $\text{TlCl}$  at  $9.2 \cdot 10^{-5}$  M shows that the process is quite fast and that equilibrium is reached after 2 hours (Fig. S3, ESI). The adsorption isotherm conducted at room temperature is shown in Fig. 4S, ESI. The curve is concave relative to the concentration axis, which reflects the strong affinity of the NPs for the  $\text{Tl}^+$  sorption in a wide range of concentration. The maximum adsorption capacity ( $Q_{\text{max}}$ ), which is indicative of the efficiency of the materials to capture thallium ion determined from the plateau of the isotherms is equal to 26.6 wt%. It corresponds to the adsorption of 0.5 mole of  $\text{Tl}^+$  per mole of iron. The curve is linear at low concentrations indicating that all of the  $\text{Tl}^+$  is inserted into the cyano-bridged network. The structural integrity of PB NPs after  $\text{Tl}^+$  adsorption was confirmed by IR and PXRD analysis of isolated  $^{201}\text{Tl}^+$ /PB@stabilizer NPs whose chemical composition was determined by elementary analysis and corresponds to the formulas  $\text{Tl}_{0.61}\text{Fe}[\text{Fe}(\text{CN})_6]_{0.90} @ (\beta\text{-GluTEG-NH}_2)_{0.60}$  and  $\text{Tl}_{0.58}\text{Fe}[\text{Fe}(\text{CN})_6]_{0.89} @ (\text{PEG-NH}_2)_{0.20}$ . Both show a stretching vibration of cyano groups and lattice parameters similar before and after thallium capture (see respectively ESI and Fig. 1S). The TEM images also show that no change in the textural aspects of the NPs was observed after  $\text{Tl}^+$  insertion (Fig. 5S, ESI). Leaching test of  $\text{Tl}^+$  performed for these NPs in aqueous solution at physiological pH for 48 h confirmed their stability without significant loss of  $\text{Tl}^+$  (see ESI).

A toxicity study prior to the use of these NPs in SPECT/CT was performed.<sup>11</sup> MTT assays which determine the cell metabolic activity

in the mitochondria of viable cells<sup>32</sup> were conducted with fibroblast BALB/c 3T3 cells and undifferentiated embryonic stem cells D3. We selected these cell lines as model systems because the use of cells from different embryonic origins is an important approach to understand the cell-specific responses induced by NPs.<sup>33</sup> Cell viability of exposure to PB@stabilizer NPs was calculated as the percentage of tetrazolium salt reduction by viable cells in each sample and the values were normalised by the untreated cell control. It was expressed in terms of its IC<sub>50</sub> (the concentration causing 50% death of the cell population) calculated from concentration–response curves using SPSS software.<sup>34</sup> A MTT assay for short period of exposure (48 h) to the BALB/c 3T3 cells and a long period exposure (10 days) to the BALB/c 3T3 cells and D3 were carried out. For Na<sub>0.45</sub>Fe[Fe(CN)<sub>6</sub>]<sub>0.86</sub>@(PEG-NH<sub>2</sub>)<sub>0.22</sub> NPs, the IC<sub>50</sub> of short exposure corresponds to 1380 µg/mL of nanoparticles (1064–4993 µg/mL). The IC<sub>50</sub> for 3T3 cells for long exposure was 370 µg/mL (163–1849 µg/mL), while for D3 cell line this value was 275 µg/mL (119–2088 µg/mL). To evaluate the genotoxicity of NPs, the Comet assay was also carried out.<sup>35</sup> It consists of extracting and running an electrophoresis of the single cells' DNA, and measuring the amount of DNA that migrates (tail) for each nucleoid. The migrated fragments indicate the damage in the genetic material. After analysis of results, no biological effects was observed for the investigated nanoparticles (Fig. 6S, ESI). Up & Down acute toxicity test was carried out by intravenous (*iv*) administration of a single dose of 137 mg/Kg Na<sub>0.45</sub>Fe[Fe(CN)<sub>6</sub>]<sub>0.86</sub>@(PEG-NH<sub>2</sub>)<sub>0.22</sub> NPs. No mortality was achieved into the 48h post administration and LD<sub>50</sub> (median lethal dose) was considered to be greater than 137 mg/Kg. Necropsy of the treated animals did not reveal any alteration. Blood sample was collected prior to euthanasia in order to check hematology and leukocyte profile. Haematology revealed a slight decrease in white blood cells, but no imbalance in the leukocyte profile was observed (Tables 1S & 2S, ESI). Despite the data from Up & Down acute toxicity assay, which reflects that no mortality can be achieved, the haematology results suggest a repeat dose study to verify the results. Note also that the quantity of *iv* injected NPs for *in vivo* SPECT/CT imaging corresponds to 7.5 mg/Kg far below the quantity injected for the toxicity tests. In order to use <sup>201</sup>Tl-labelled NPs as tracking agents for *in vivo* SPECT/CT imaging, sodium-containing PB@PEG-NH<sub>2</sub> and PB@β-GluTEG-NH<sub>2</sub> NPs (1 mg of NPs in 500 µL of a 0.9 % NaCl aqueous solution) were mixed with a <sup>201</sup>TlCl aqueous solution having an activity of 10 MBq.mL<sup>-1</sup> to obtain <sup>201</sup>Tl<sup>+</sup>/PB@PEG-NH<sub>2</sub> and <sup>201</sup>Tl<sup>+</sup>/PB@β-GluTEG-NH<sub>2</sub> nanoprobes, respectively. These radio-labelled NPs (8 MBq) were *iv* injected into the tail vein of mice and the SPECT/CT images were acquired at different times during 48 h. Representative images of mice after the *iv* injection of <sup>201</sup>Tl<sup>+</sup>/PB@PEG-NH<sub>2</sub> at different time periods from 20 min to 48 h are shown in Fig. 2. The 3D quantification by segmentation using dedicated software (Inviscope®) was performed in order to recover the information about *in vivo* uptake by organs. Maximum Intensity Projections (MIPs) images of the longitudinal plane (Fig. 2a) as well as the transversal planes of the organs of interest (Fig. 2b-d) demonstrate the transient passage of the radio-labelled NPs successively into the lungs (after 1h 20min), liver (after 3h20min) and then the kidneys. This biodistribution is clearly different in comparison to the commercial <sup>201</sup>TlCl used as a reference standard, which is located immediately in

the kidney (Fig. 7S, ESI). Faster transient passage through the pulmonary compartment was observed in the SPECT/CT images obtained using the radio-labelled <sup>201</sup>Tl<sup>+</sup>/PB@β-GluTEG-NH<sub>2</sub> nanoprobes before their clearance by natural means (liver and kidneys) (Fig. 8S, ESI). In this case, the NPs were localised in the lungs for the first 20 min before being transferred to the liver. To compare data from different animals and to overcome the heterogeneity of *iv* injections, quantifications data were normalized and the recorded activity of the whole body was considered to be 100 % for each acquisition. The uptake kinetics by the organs of interest (bladder, lungs, kidneys, liver) at different times after a single *iv* dose of nanoprobes <sup>201</sup>Tl<sup>+</sup>/PB@PEG-NH<sub>2</sub> and <sup>201</sup>Tl<sup>+</sup>/PB@β-GluTEG-NH<sub>2</sub> as well as for commercial radiotracer <sup>201</sup>TlCl are shown in Fig. 3 and Fig. 9S.

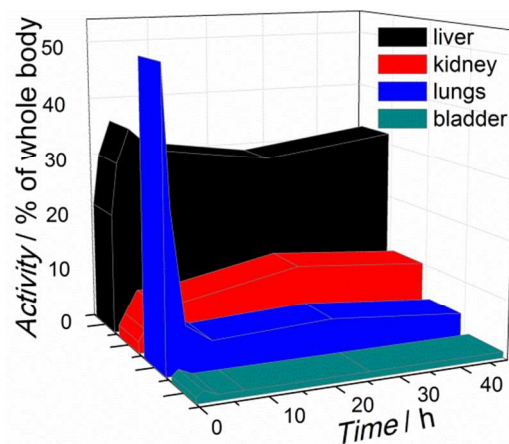


**Figure 3.** Captation of <sup>201</sup>Tl-labelled nanoparticles <sup>201</sup>Tl<sup>+</sup>/PB@PEG-NH<sub>2</sub> by organs of interest in times after *iv* injection.

Comparative data confirm the difference observed between the two nanoprobes. Thus, the PEG-enwrapped NPs, <sup>201</sup>Tl<sup>+</sup>/PB@PEG-NH<sub>2</sub>, show a high activity in the lungs for the first 2h with a subsequent pass through the liver and in the kidneys. In contrast, the sugar-enwrapped NPs, <sup>201</sup>Tl<sup>+</sup>/PB@β-GluTEG-NH<sub>2</sub>, are massively retained in the liver from beginning even if another part will reside in the lungs for a short time of about 20 min and in the kidneys with a gradual elimination over a comparable time as in the previous case. The sugar-enwrapped NPs <sup>201</sup>Tl<sup>+</sup>/PB@β-GluTEG-NH<sub>2</sub> are therefore unable just after injection to cross in whole the liver barrier in contrast to PEG-enwrapped NPs. To evaluate the elimination of the <sup>201</sup>Tl<sup>+</sup> entrapped in Prussian Blue NPs and compare to that of the commercial radiotracer, SPECT activity was recorded during 48h post *iv* injection. The excretion from the body by glomerular filtration is operational for the three radiotracers *i.e.* both studied Prussian Blue-based NPs and commercial <sup>201</sup>TlCl as attested by the whole activity curve vs time (Fig. 4). The biological half-life was estimated to be 36h for <sup>201</sup>Tl<sup>+</sup> trapped in the NPs, which is in the same range from that observed for the injection of an aqueous solution of <sup>201</sup>TlCl equal to 34h.

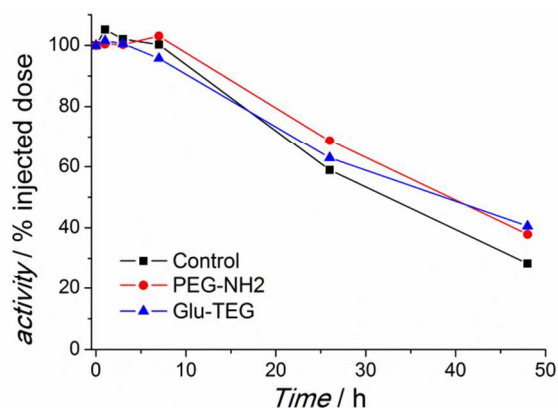


**Figure 4.** Elimination kinetic curves for  $^{201}\text{Tl}$ -labeled nanoparticles  $^{201}\text{Tl}^+$ /PB@ $\beta$ -GluTEG-NH<sub>2</sub> (-▲-) and  $^{201}\text{Tl}^+$ /PB@ $\beta$ -GluTEG-NH<sub>2</sub> (-●-) as well as for the commercial  $^{201}\text{TlCl}$  (-■-).

In conclusion, we synthesized in aqueous solution ultra-small (2–3 nm) Prussian blue NPs stabilized with biocompatible amino PEG or glucose functionalized aminotriethyleneglycol ligands that can be readily labelled with non-radioactive or radioactive ( $^{201}\text{Tl}^+$ ) thallium isotopes. *In vivo* SPECT/CT imaging thereof shows that these nanoproboscopes present a transient pass in the pulmonary compartments and then in the liver being also excreted by glomerular clearing. This study shows that the distribution in time of the  $^{201}\text{Tl}^+$ -radiotracer when inserted within a nanoparticle differs greatly from that of the commercial  $^{201}\text{TlCl}$  salt and is also dependent on the surface functionalization of the nanoparticle. Besides, the biological half-life of  $^{201}\text{Tl}^+$  trapped in these nanoproboscopes is similar to that of the commercial radiotracer  $^{201}\text{TlCl}$ . This study is the first example of *post iv* injection SPECT/CT monitoring of coordination polymer NPs on the small animal. It may also be viewed as the first step toward the design of new SPECT/CT imaging radio nanoproboscopes based on Prussian blue NPs that can be used for imaging of the lungs and liver.

## Acknowledgements

The authors thank the ERA.NET-RUS project ST085 COPONAMRI, University of Montpellier II and CNRS for financial support. We also thank D. Granier (PAC Chimie Balard, Montpellier) for PXRD measurements and Dr. M. Gary-Bobo (IBMM, UM1) for helpful discussion.

## Notes and references

- <sup>a</sup> Institut Charles Gerhardt Montpellier (ICGM), UMR 5253, Chimie Moléculaire et Organisation du Solide, Université Montpellier 2, place Eugène Bataillon, Montpellier, France. E-mail: [joulia.larionova@um2.fr](mailto:joulia.larionova@um2.fr)  
<sup>b</sup> Institut de Recherche en Cancérologie de Montpellier (IRCM), INSERM, U896, Université Montpellier 1, Montpellier, France. E-mail: [muriel.busson@inserm.fr](mailto:muriel.busson@inserm.fr)  
<sup>c</sup> Service de Médecine Nucléaire, Centre Hospitalier Universitaire Nîmes, INSERM U896, Université Montpellier 1, Montpellier, France.

<sup>d</sup> Institut des Biomolécules Max Mousseron (IBMM), UMR 5247, Nucléosides et Effecteurs Phosphorylés, Université Montpellier 2, place Eugène Bataillon, Montpellier, France.

<sup>e</sup> PCB\_Unit of Experimental Toxicology and Ecotoxicology (UTOX-PCB), Scientific Park of Barcelona 08028, Spain.

Electronic Supplementary Information (ESI) available: experimental details and procedures, toxicological data, PXRD, TEM images, kinetics and adsorption isotherms, SPECT/CT images,  $\text{Tl}^+$  captation profiles. See DOI: 10.1039/c000000x/

- 1 a) O. Hatlevik, W. E. Buschmann, J. Zhang, J. L. Manson and J. S. Miller, *Adv. Mater.*, 1999, **11**, 914; b) S. M. Holmes and G. S. Girolami, *J. Am. Chem. Soc.*, 1999, **121**, 5593; c) W. R. Entley and G. S. Girolami, *Science*, 1995, **268**, 397; d) S. Ferlay, T. Mallah, R. Ouahes, P. Veillet and M. Verdaguer, *Nature*, 1995, **378**, 701; e) V. Gadet, T. Mallah, I. Castro and M. Verdaguer, *J. Am. Chem. Soc.*, 1992, **114**, 9213; f) T. Mallah, S. Thiebaut, M. Verdaguer and P. Veillet, *Science*, 1993, **262**, 1554; g) O. Sato, T. Iyoda, A. Fujishima and K. Hashimoto, *Science*, 1996, **271**, 49; h) S. Ohkoshi and K. Hashimoto, *J. Am. Chem. Soc.*, 1999, **121**, 10591; i) R. Koncki, *Crit. Rev. Anal. Chem.*, 2002, **32**, 79.
- 2 a) L. Roberts, *Science*, 1987, **238**, 1028; a) P. A. Haas, *Sep. Sci. Technol.*, 1993, **28**, 2479; b) J. Lehto and L. Szirtes, *Radiat. Phys. Chem.*, 1994, **43**, 261; c) H. Mimura, J. Lehto and R. Harjula, *J. Nucl. Sci. Technol.*, 1997, **34**, 607; d) R. Harjula, J. Lehto, A. Paajanen, L. Brodtkin and E. Tusa, *Nucl. Sci. Eng.*, 2001, **137**, 206; e) R. Harjula, J. Lehto, A. Paajanen, E. Tusa and P. Yarnell, *React. Funct. Polym.*, 2004, **60**, 85; f) D. Wenker, B. Spiess, P. Laugel, *Food Addit. Contam.*, 1990, **7**, 375; g) S. Ayrault, C. Loos-Neskovic, M. Fedoroff, E. Garnier, *Talanta*, 1994, **41**, 1435.
- 3 a) J. Larionova, Y. Guari, C. Sangregorio, C. Guérin, *New J. Chem.* 2009, **33**, 1177; b) E. Dujardin, S. Mann, *Adv. Mater.* 2004, **16**, 1125; c) S. Vaucher, M. Li, S. Mann, *Angew. Chem. Int. Ed.*, 2000, **39**, 1793; d) S. Mann, J. Fielden, M. Li, E. Dujardin and S. Mann, *Nano Lett.*, 2002, **2**, 225; e) T. Uemura and S. Kitagawa, *J. Am. Chem. Soc.*, 2003, **125**, 7814; f) D. Brinzei, L. Catala, C. Mathonière, W. Wensdorfer, A. Gloter, O. Stephan and T. Mallah, *J. Am. Chem. Soc.*, 2007, **129**, 3778; g) D. Asakura, C. H. Li, Y. Mizuno, M. Okubo, H. Zhou and D. R. Talham, *J. Am. Chem. Soc.*, 2013, **135**, 2793; h) L. Catala, D. Brinzei, Y. Prado, A. Gloter, O. Stéphan, G. Rogez and T. Mallah, *Angew. Chem. Int. Ed.*, 2009, **48**, 183; h) Y. Prado, N. Dia, L. Lisnard, G. Rogez, F. Brisset, L. Catala and T. Mallah, *Chem. Commun.*, 2012, **48**, 11455; i) G. Maurin-Pasturel, J. Long, Y. Guari, F. Godiard, M.-G. Willinger, C. Guérin and J. Larionova, *Angew. Chem. Int. Ed.*, 2014, **53**, 3872; j) N. L. Torad, M. Hu, M. Imura, M. Naito, Y. Yamauchi, *J. Mater. Chem.*, 2012, **22**, 18261; k) M. Hu, A. A. Belik, M. Imura, Y. Yamauchi, *J. Am. Chem. Soc.*, 2013, **135**(1), 384; l) M. Hu, S. Ishihara, K. Ariga, M. Imura, Y. Yamauchi, *Chemistry - A European Journal*, 2013, **19** (6), 1882.
- 4 a) M. Shokouhimehr, E. S. Soehnlen, A. Khitrin, S. Basu and S. D. Huang, *Inorg. Chem. Commun.*, 2010, **13**, 58; b) M. Shokouhimehr, E. S. Soehnlen, H. H. Hao, M. Griswold, C. Flask, X. D. Fan, J. P. Basilion, S. Basu and S. P. D. Huang, *J. Mater. Chem.*, 2010, **20**, 5251; c) S. D. Huang, Y. Li, M. Shokouhimehr, US Patent WO 2011/106309 A2, 2011; d) S. D. Huang, A. K. Khitrin, V. S. Perera, patent WO 2012/108856 A1, 2012; e) S. D. Huang, Y. Li, M. Shokouhimehr, US Patent US20090384391 20090403, 2010; f) Y.

- Guari, J. Larionova, M. Corti, A. Lascialfari, M. Marinone, G. Poletti, K. Molvinger and Ch. Guérin, *Dalton Trans.*, 2008, 3658; g) E. Chelebaeva, J. Larionova, Y. Guari, R. A. S. Ferreira, L. D. Carlos, A. A. Trifonov, T. Kalaivani, A. Lascialfari, Ch. Guérin, K. Molvinger, L. Datas, M. Maynadier, M. Gary-Bobo and M. Garcia, *Nanoscale*, 2011, **3**, 1200; h) M. Perrier, S. Kenouche, J. Long, T. Kalaivani, J. Larionova, Ch. Goze-Bac, A. Lascialfari, M. Mariani, N. Baril, Ch. Guérin, B. Donnadiou, A. Trifonov and Y. Guari, *Inorg. Chem.*, 2013, **52**, 13402; i) G. Paul, Y. Prado, N. Dia, E. Rivière, S. Laurent, M. L. Vander Elst, R. N. Muller, L. Sancey, P. Perriat, O. Tillement, T. Mallah and L. Catala *Chem. Commun.*, DOI:10.1039/c4cc01251h; j) M. F. Dumont, H. A. Hoffman, P. R. S. Yoon, L. S. Conklin, S. R. Saha, J. P. Paglione, R. W. Sze and R. Fernandes, *Bioconjugate Chemistry*, 2014, **25**, 129.
- 5 a) V. S. Perera, J. Hao, M. Gao, M. Gough, P. Y. Zavalij, C. Flask, J. P. Basilion and S. D. Huang, *Inorg. Chem.*, 2011, **50**, 7910.
- 6 a) S. Ye, Y. Liu, S. Chen, S. Liang, R. McHale, N. Ghasdian, Y. Lu and X. Wang, *Chem Commun.*, 2011, **47**, 6831.
- 7 G. Fu, W. Liu, S. Feng and X. Yue, *Chem. Commun.*, 2012, **48**, 11567.
- 8 a) H. F. Weich, H. W. Strauss and B. Pitt, *Circulation*, 1977, **56**, 188; b) E. Lebowitz, M. W. Greene, R. Fairchild, P. R. Bradely-Moore, H. L. Atkins, A. N. Ansari, P. Richards and E. Belgrave, *J. Nucl. Med.*, 1975, **15**, 151.
- 9 P. J. Kulesza, M. A. Malik, A. Denca and J. Strojek, *J. Anal. Chem.*, 1996, **68**, 2442.
- 10 H. J. Buser, D. Schwarzenbach, W. Petter and A. Ludi, *Inorg. Chem.*, 1977, **16**, 2705.
- 11 H. – Y. Lian, M. Hu, C.-H. Liu, Y. Yamauchi, K. C.-W. Wu, *Chem. Commun.*, 2012, **48**, 5151.
- 12 a) D. R. Nogueira, M. del Carmen Morán, M. Mitjans, L. Pérez, D. Ramos, J. de Lapuente and M. Pilar Vinardell, *Nanotoxicology*, 2014, **8**, 404; b) M. Rodrigues, A. C. Calpena, D. B. Amabilino, D. Ramos-López, J. de Lapuente and L. Pérez-García, *RSC Adv.*, 2014, **4**, 9279; c) I. Giannicchi, R. Brisso, D. Ramos, J. de Lapuente, J. C. Lima, A. Dalla Cort and L. Rodríguez, *Inorg Chem.*, 2013, **52**, 9245.
- 13 C. S. Paim, D. R. Nogueira, M. Mitjans, D. Ramos Lopez, J. de Lapuente Perez, M. Steppe, E. E. Schapoval and M. P. Vinardell, *Photochem Photobiol Sci.*, 2013, **12**, 805.
- 14 SPSS version 16, SPSS Inc., Chicago, Illinois, USA.
- 15 L. de Marzi, A. Monaco, J. de Lapuente, D. Ramos, M. Borrás, M. di Gioacchino, S. Santucci and A. Poma, *Int. J. Mol. Sci.*, 2013, **14**, 3065.